Journal of Nanophotonics

SPIEDigitalLibrary.org/jnp

Structural optimization of quantum wells used in a 1-μm vertical-external-cavity surface-emitting laser

Peng Zhang
Yanrong Song
Teli Dai
Yiping Liang

SPIE

Structural optimization of quantum wells used in a 1-μm vertical-external-cavity surface-emitting laser

Peng Zhang,[a,b] Yanrong Song,[c] Teli Dai,[a,b] and Yiping Liang[a,b]

[a] Chongqing Normal University, College of Physics and Electronic Engineering, Tian Chen Road, Chongqing 400047, China

[b] Chongqing Normal University, Chongqing Key Laboratory of Optical Engineering, Chongqing 400047, China

[c] Beijing University of Technology, College of Applied Sciences, Beijing 100124, China

gchzh2003@yahoo.com.cn

Abstract. On the basis of the analysis of material gain, a comprehensive optimization of quantum wells used in a 1-μm vertical-external-cavity surface-emitting laser was carried out. For a single-well structure, the optimized width lies between 8 and 10 nm, the optimized depth is a quantum well with ~0.1 Al composition in AlGaAs barrier, and the optimized configurations are graded-index quantum well and quantum well with AlGaAs barrier and a GaAs buffer layer. The optimal width of a double- or triple-well structure lies between 6 and 8 nm. Compared to its single- and triple-well counterparts, double-well structure provides higher gain and has more tolerance to the deviation of laser wavelength. [DOI: 10.1117/1.3562569]

Keywords: vertical-external-cavity surface-emitting lasers; quantum wells; material gain.

Paper 10086LR received Nov. 24, 2010; revised manuscript received Jan. 27, 2011; accepted for publication Feb. 1, 2011; published online Apr. 5, 2011.

1 Introduction

Optically pumped vertical-external-cavity surface-emitting lasers (VECSELs), which replace the top distributed Bragg reflector of vertical-cavity surface-emitting lasers by a external cavity mirror and use optical pumping instead of electrical pumping, are attractive and under intensive study in recent years due to their power scalability, beam quality, and flexible spectral coverage.[1] High output power and good beam quality 1-μm VECSELs have many applications in frequency conversion,[2] energy utilization,[3] and optical spectroscopy.[4]

To obtain a more efficient or higher output power VECSEL, the elaborate design of quantum wells (QWs) is primary and necessary. Moloney et al.[5] and Hader et al.[6] have presented overviews of a novel first-principle quantum approach to design semiconductor QW for target wavelength. In this paper, we demonstrate a structural optimization of QWs that is mainly based on the analysis of material gain. We optimize the single-well structure according to the width, depth, and configuration dependences of the material gain, and then the double well (first introduced in a VECSEL by Fan et al.[7]) and triple well (have been experimentally used by Yoo et al.[8] and Schulz et al.[9]) structures are compared and optimized.

The theoretical model is quite straightforward. First, we use the famous $k \cdot p$ method to calculate the band structures. The Hamiltonian of electrons in a conduction band (CB) is

$$H^c(k) = \frac{\hbar^2}{2}\left(\frac{\boldsymbol{k}_t^2}{m_e^t} + \frac{\boldsymbol{k}_z^2}{m_e^z}\right) + V_e(z) + E_{hc}, \tag{1}$$

where the wave vector $\boldsymbol{k}$ is interpreted as a differential operator $-i\nabla$ and the transverse wave vector $\boldsymbol{k}_t = \boldsymbol{k}_x + \boldsymbol{k}_y$, m_e^t, and m_e^z are the electron effective masses perpendicular (t) and parallel

1934-2608/2011/$25.00 © 2011 SPIE

(z) to the growth direction, $V_e(z)$ is the potential energy of the unstrained conduction band edge. The CB structure can be determined by solving $H^c\phi_n(z) = E_n^c\,\phi_n(z)$ at $\boldsymbol{k}_t = 0$, then the parabolic approximation is used to obtain the whole CB structure and the envelope functions.

The 6×6 Luttinger–Kohn Hamiltonian,[10] in which the heavy-hole, light-hole, and spin-orbit coupling are taken into account, is used to obtain the valence band (VB) structures of the QW. The envelope function and the subband energy of VB in a QW can be obtained by solving the multiband effective mass equation,

$$\sum_m \left[H^{vv'}\left(\boldsymbol{k}_t, -i\frac{d}{dz}\right) + V_h(z)\right] g_m^{v'}(\boldsymbol{k}_t, z) = E_m^v g_m^v(\boldsymbol{k}_t, z), \tag{2}$$

where $V_h(z)$ is the potential of the hole and $V_e(z) = V_h(z)+E_g$. For bandgap E_g, the increasing temperature caused bandgap reduction is $E_g(T) = E_g(0) - \alpha\Theta\{[1 + (2T/\Theta)^p]^{1/p}\text{-}1\}/2$, where $E_g(0)$ is the bandgap under 0 K, α is the slope parameter, Θ and p are the average phonon temperature and the phonon dispersion parameter. The Coulomb interaction is taken into account through the bandgap renormalization formula derived from many-body theory,[11,12]

$$\Delta E_g = -C\left[\frac{\varepsilon_{st}^5}{N}\left(m_0\frac{m_c + m_v}{m_c m_v} + BT^2\frac{\varepsilon_{st}}{N}\right)\right]^{-1/4}, \tag{3}$$

where ε_{st} is the static dielectric, m_c and m_v are effective masses, T and N are temperature and carrier density, C and B are two fit parameters. This simplification was found in good agreement with reported experimental results[13] and is suitable for the optimization of the QW structure, which is rather qualitative and not as rigorous as accurate design demands.

Then, the material gain of a QW is[10,14]

$$g(\hbar\omega) = \frac{\pi q^2}{n_w c\varepsilon_0 m_0^2 \omega L_w}\sum\int |\vec{e}\cdot M_{nm}(k_t)|^2 \frac{\left[f_n^c(\boldsymbol{k}_t) - f_m^v(\boldsymbol{k}_t)\right]\gamma/\pi}{\left[E_{nm}^{cv}(\boldsymbol{k}_t) - \hbar\omega\right]^2 + \gamma^2}\frac{\boldsymbol{k}_t d\boldsymbol{k}_t}{2\pi}, \tag{4}$$

where q and m_0 are the electron charge and rest mass, c and ε_0 are the velocity of light and the permittivity in free space, n_w and L_w are the refractive index and the width of the QW, γ is the half linewidth of the Lorentzian function, $M_{nm}(\boldsymbol{k}_t)$ is the momentum matrix element, $f_n^c(\boldsymbol{k}_t)$ and $f_m^v(\boldsymbol{k}_t)$ are the Fermi distribution functions, and $E_{nm}^{cv}(\boldsymbol{k}_t)$ is the transition energy.

For strained QWs, the strain-induced hydrostatic deformation potential (E_{hc} in CB and E_{hv} in VB) and the tetragonal distortion energy (E_t) are included, the band offsets are calculated using model-solid theory, and all parameters of ternary alloy ABC are obtained by the interpolation of related binary material AB and AC as $P(AB_xC_{1-x}) = xP(AB) + (1-x)P(AC) - x(1-x)b_{ABC}$, where b_{ABC} is the bowing parameter of ternary alloy ABC, which indicates the deviation from the linear interpolation. Details for the numerical computation and parameters used in the calculation can be found in Refs. 10,11, and 13.

2 Optimization of a Single-Well Structure

In the following, we will discuss the influences of the width, depth, and configuration of the QWs on the material gain. In the calculation, the QWs are all $In_{0.132}Ga_{0.868}As$ for operating near 1-μm wavelength, the carrier density is assumed to be a representative number of 3.6×10^{24} m^{-3} and the temperature to be 300 K except we have a special note.

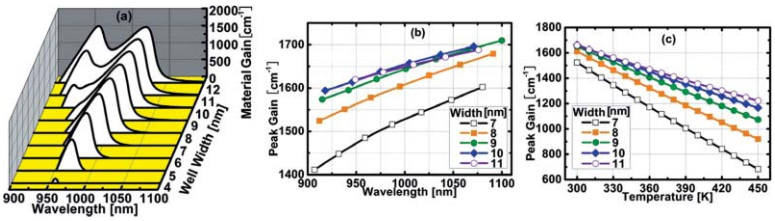

Fig. 1 (a) Gain spectra, (b) peak gains as functions of emission wavelengths, and (c) peak gains versus temperature of the single-well structures with different width.

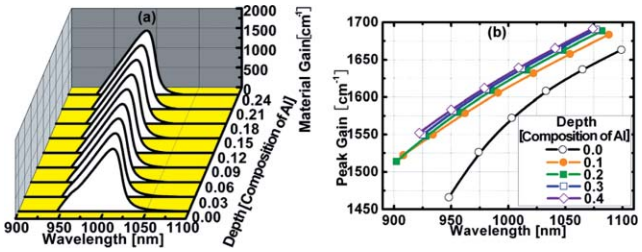

Fig. 2 (a) Gain spectra and (b) peak gains as functions of emission wavelengths of the single-well structures with different depth.

2.1 *QW Width*

Figure 1(a) shows the width dependence of material gain of a single-well structure (with $Al_{0.06}Ga_{0.94}As$ barrier). It can be seen that, when the width is <8 nm, although the narrower width brings stronger quantum confinement, thus, more intensive envelope function, the overlapping integration in transition matrix element still decreases because of the decreased integral domain. This leads to a significant reduction of material gain. When the width is >10 nm, the quantum confinement becomes weaker; the second confined level of electrons appears, and the gain spectrum becomes wider and with a subpeak.

When the composition of In in InGaAs QW is changed, the corresponding emission wavelength and peak gain are also changed. We plot the peak gains as functions of the emission wavelengths of QWs with different width in Fig. 1(b). It is quit clear that the optimal width is from 8 to 10 nm because the peak gain of QW of <8 nm is much smaller, and the peak gain of QW of >10 nm begins to decrease.

Figure 1(c) shows the relationship between the peak gain and temperature. As can be seen, the wider wells have better temperature stability. Because wells of <8 nm are very sensitive to the temperature and the improvement of the stability is not clear when the width exceeds 10 nm, the optimal width is 8–10 nm, when the temperature stability is considered.

2.2 *QW Depth*

The depth-dependence of material gain of a single-well structure is shown in Fig. 2(a) (the well width is assumed to be 8 nm, and the composition of Al in AlGaAs barrier is chosen to characterize the depth). The influence of the depth on the emission wavelength is obvious: the emission wavelength blueshifts of $\sim$20nm when the Al composition changes from 0 to 0.24. However, the affect of the depth on the peak gain is not clear: the peak gain increases only $\sim$2% when the Al composition varies from 0 to 0.24.

Changing Al composition of AlGaAs barrier, we plot the curves of peak gain versus emission wavelengths in Fig. 2(b). It shows that QWs with AlGaAs barriers have bigger gain than with GaAs (i.e., zero Al composition) barrier, and 0.1 composition of Al is enough because the contribution of more Al composition to the increase of gain is not clear.

2.3 *QW Configuration*

As shown in Fig. 3, we consider six different QW configurations, which are generally used in InGaAs strained QW VECSELs. Figure 4(a) shows the gain spectra of the above six

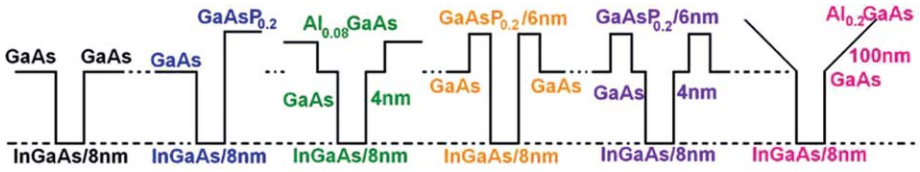

Fig. 3 Configurations of six different single-well structures.

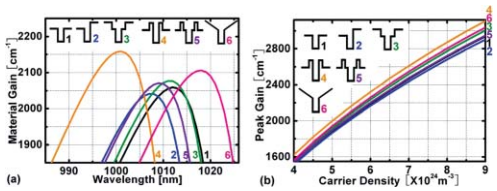

Fig. 4 (a) Gain spectra and (b) peak gains versus carrier density of six different single-well structures.

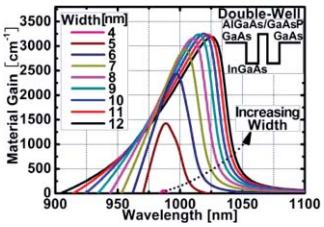

Fig. 5 Gain spectra of double-well structures with different width.

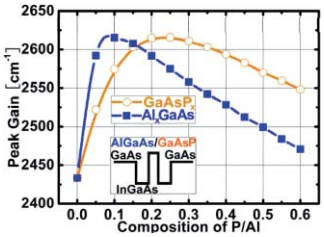

Fig. 6 Influence of P/Al composition on peak gain in double-well structure.

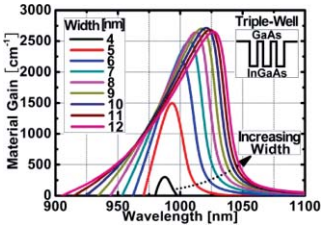

Fig. 7 Gain spectra of different triple-well structures.

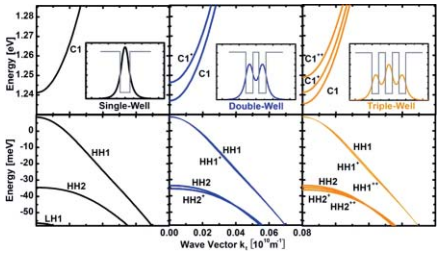

Fig. 8 Band structures of single-, double-, and triple-well structures.

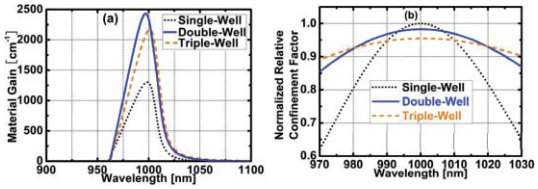

Fig. 9 (a) Comparison of gain and (b) confinement factors of single-, double-, and triple-well structures.

different QWs (the carrier density is assumed to be 4.6×10^{24} m^{-3}). We can see that the fourth QW has the largest peak gain and the shortest emission wavelength because of its deepest well depth, while the last QW has the secondary peak gain and the longest emission wavelength.

Figure 4(b) indicates the peak gains of six different single-well structures versus carrier density. Except for the fourth QW, which always has bigger peak gain, the contrast of the peak gains of the other five QWs is not evident when the carrier density is small. However, when the carrier density is increased, differences of the other five QWs are expanded, and the third and last QWs excel the rest, obviously, and this is in good agreement with reported experiment.[15] Considering that GaAsP layer in the fourth QW may block the carriers diffusing to the well, we recommend the third and last QWs for high-power VECSELs.

3 Optimization of a Double-Well Structure

The gain spectra of double-well structure with different width are shown in Fig. 5 (the width means the width of every individual well; the spacer is 6 nm $GaAs_{0.94}P_{0.06}$). It can be concluded from Fig. 5 that the optimal width of a double-well structure is from 6 to 8 nm.

Generally, the spacer between two separated wells can be GaAs, AlGaAs, or GaAsP. When AlGaAs or GaAsP is used as the spacer, the Al/P composition will affect the gain. Figure 6 shows the influence of Al/P composition on the peak gain of a 6-nm double-well structure. We can see from Fig. 6 that AlGaAs/GaAsP spacer is better than GaAs spacer (i.e., zero Al/P), and the optimal compositions of Al or P are about 0.08 and 0.2, respectively.

4 Optimization of a Triple-Well Structure

The width dependence of gain of a triple-well structure is shown in Fig. 7 (the meaning of the width is same as in double-well structure). Because excessively high spacer will block the carriers diffusing to the middle well, the spacers are assumed to be 6 nm GaAs layer. It can be seen from Fig. 7, the optimal width of a triple-well structure is also between 6 and 8 nm.

Now we compare the single-, double-, and triple-well structures with each other. Figure 8 shows the band structure of them under same conditions: GaAs barriers, 6-nm well width, and 6-nm GaAs spacer. The inserts are their energy profiles and envelope functions of the first confined level in CB. As shown in Fig. 8, single-well structure has one confined level in CB and three confined levels in VB. For double- and triple-well structures, because of the coupling, every band splits into two and three levels, respectively, and the split separations between higher levels are clearer. This level split can be used to explain why there is no subpeak in the gain spectra of double- and triple-well structure when the width increases up to 12 nm.

Figure 9(a) shows the gain spectra of the three QW structures (6-nm width). It can be seen that a double-well structure has the largest gain, and this can partly been interpreted by the insets in Fig. 8: for the overlapping integration in the transition matrix element, single-well structure has the largest amplitude of envelope function but the smallest integral domain, while triple-well structure has the smallest amplitude of envelope function but the largest integral domain. In comparison, double-well structure has moderate amplitude of envelope function and integral domain, thus produce the largest gain.

Figure 9(b) shows the normalized confinement factors as functions of laser wavelengths. The designed operating wavelength is 1 μm. Obviously, single-well structure has the poorest tolerance: when the laser wavelength deviates from 1 μm to $\sim$10 nm, the confinement factor is decreased by 5%, and this may result in rollover of a VECSEL.

Figures 9(a) and 9(b) show that within a 20-nm deviated wavelength range, double-well structure has not only a higher gain than triple-well structure, but also a larger confinement factor than triple-well structure. Thus, if the tolerance is the main factor that needs to be considered in the design, then double-well structure seems to be enough for a 1-μm VECSEL. If taking into account the thickness of the active region, or for a long-wavelength VECSEL, triple-well, even quadruple-well structures may be an alternative.

5 Conclusions

In conclusion, on the basis of the analysis of material gain, we have presented a comprehensive structural optimization of the QWs used in a 1-μm VECSEL. For a single-well structure, the optimal width lies between 8 and 10 nm, the optimal depth is QW with ~0.1 Al composition in AlGaAs barrier, and the optimal configurations are graded-index QW and QW with AlGaAs barrier and GaAs buffer layer. The optimized width of a double- or triple-well structure lies between 6 and 8 nm. For a double-well structure, using AlGaAs with ~0.08 Al composition or GaAsP with ~0.2 P compositions as the spacer can produce the maximum peak gain. Compared to its single- and triple-well counterparts, double-well structure provides higher gain and has enough tolerance to the wavelength deviation.

References

1. A. C. Tropper and S. Hoogland, "Extended cavity surface-emitting semiconductor lasers" *Prog. Quant. Electron.* **30**, 1–43 (2006).
2. T. D. Raymond, W. J. Alford, M. H. Crawford, and A. A. Allerman, "Intracavity frequency doubling of a diode-pumped external cavity surface emitting semiconductor laser," *Opt. Lett.* **24**, 1127–1129 (1999).
3. A. Richter, E. Heumann, and G. Huber, "Power scaling of semiconductor laser pumped Praseodymium-laser,"*Opt. Express* **15**, 5172–5178 (2007).
4. A. Garnache, A. A. Kachanov, F. Stoeckel, and R. Planel, "High-sensitivity intracavity laser absorption spectroscopy with vertical-external-cavity surface-emitting semiconductor lasers," *Opt. Lett.* **24**, 826–828 (1999).
5. J. V. Moloney, J. Hader, and S. W. Koch, "Quantum design of semiconductor active materials laser and amplifier applications," *Laser Photon. Rev.* **1**, 24–43 (2007).
6. J. Hader, J. V. Moloney, M. Fallahi, L. Fan, and S. W. Koch, "Closed-loop design of a semiconductor laser," *Opt. Lett.* **31**, 3300–3302 (2006).
7. L. Fan, J. Hader, M. Schillgalies, M. Fallahi, A. R. Zakharian, J. V. Moloney, R. Bedford, J. T. Murray, S. W. Koch, and W. Stolz, "High-power optically pumped VECSEL using a double-well resonant periodic gain structure," *IEEE Photon. Tech. Lett.* **17**, 1764–1766 (2005).
8. J. Yoo, K. Kim, S. Lee, S. Lim, G. Kim, J. Kim, S. Cho, J. Lee, T. Kim, and Y. Park, "Gain structure optimization of vertical external cavity surface emitting laser at 920 nm," *Appl. Phys. Lett.* **89**, 131125 (2006).
9. N. Schulz, J. M. Hopkins, M. Rattunde, D. Burns, and J. Wagner, "High-brightness long-wavelength semiconductor disk lasers," *Laser Photon. Rev.* **2**, 160–181 (2008).
10. C. S. Chang and S. L. Chuang, "Modeling of strained quantum-well lasers with spin-orbit coupling," *IEEE J. Sel. Top. Quant.* **1**, 218–229 (1995).
11. R. Zimmermann, *Many-Particle Theory of Highly Excited Semiconductors*, Teubner Verlagsgesellschaft, Leipzig (1998).
12. J. Piprek, *Semiconductor Optoelectronic Devices Introduction to Physics and Simulation*, Academic Press, New York (2003).
13. P. Zhang, Y. Song, J. Tian, X. Zhang, and Z. Zhang, "Gain characteristics of InGaAs strained quantum wells with GaAs, AlGaAs and GaAsP barriers in vertical-external-cavity surface-emitting lasers," *J. Appl. Phys.* **105**, 053103 (2009).
14. E. A. Avrutin, I. E. Chebunina, I. A. Eliachevitch, S. A. Gurevich, M. E. Portnoi, and G. E. Shtengel, "TE and TM optical gains in AlGaAs/GaAs single-quantum-well lasers," *Semicond. Sci. Technol.* **8**, 80–87 (1993).
15. F. Saas, V. Talalaev, U. Griebner, J. W. Tomm, M. Zorn, A. Knigge, and M. Weyers, "Optically pumped semiconductor disk laser with graded and step indices," *Appl. Phys. Lett.* **89**, 151120 (2006).